Supporting Information

Colossal Room-Temperature Electrocaloric Effect in Ferroelectric Polymer Nanocomposites Using Nanostructured Barium Strontium Titanates

Guangzu Zhang,[†,§,#] Xiaoshan Zhang,[†,‡,#] Tiannan Yang[†], Qi Li,[†] Long-Qing Chen,[†] Shenglin Jiang,[§] and Qing Wang[†]

[†]Department of Materials Science and Engineering, The Pennsylvania State University, University Park, Pennsylvania 16802 [§]School of Optical and Electronic Information, Huazhong University of Science and Technology, Wuhan, Hubei 430074 China [‡]College of Materials Science and Engineering, Sichuan University, Chengdu 610064 China

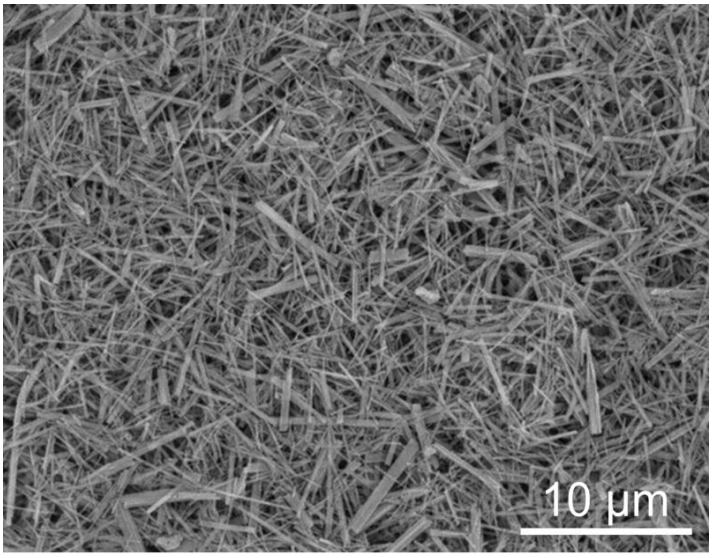

Figure S1. SEM image of the sodium titanate NW templates.

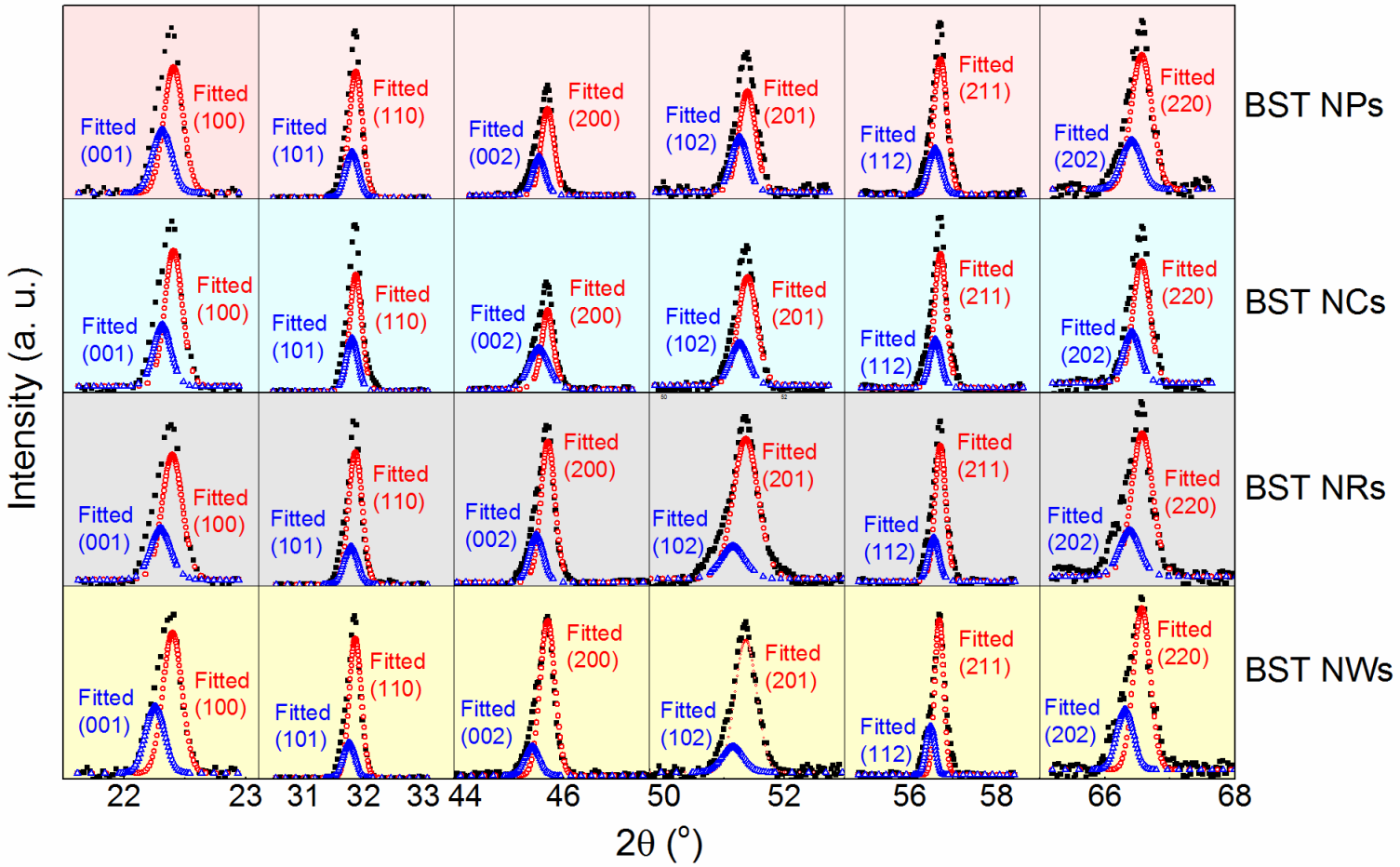

Figure S2. Detailed diffraction profiles of the XRD patterns of the BST nanoparticles (NPs), nanocubes (NCs), nanorods (NRs) and nanowires (NWs). The fitted peaks are obtained by the best fit to a mixed Gaussian-Lorentzian distribution.[1]

Table S1. Position of the characteristic peaks in the XRD patterns of the BST NPs, NCs, NRs and NWs obtained from Figure S2, and the lattice constants calculated from each peak by the Bragg equation $\lambda=2d\sin\theta$, in which λ is the X-ray wavelength (λ=1.54 Å in this work), d is the interplanar spacing, h, k and l are the Miller indices. For tetragonal BST, $d=1/\left(\sqrt{\frac{h^2+k^2}{a^2}+\frac{l^2}{c^2}}\right)$. For powders, accurate lattice constants cannot be obtained by just using Bragg equation, because of (i) the absorption of the x-ray beam in the specimen, and (ii) the displacement of the rotation axis of the specimen relative to the geometric center of the cylindrical film, usually called the eccentricity error. In this work, the relatively accurate lattice constants are derived by using an extrapolation method.[2] After calculating the lattice constants from each XRD characteristic peak by the Bragg equation, and plotting the lattice constants as a function of $\frac{1}{2}(\cos^2\theta/\theta+\cos^2\theta/\sin\theta)$, the relatively accurate lattice constants of the powders can be extrapolated at the intersection points of the ordinate axis and the linearly fitted line of the Bragg-equation calculated lattice constants. Figure S3 plots the calculated lattice constants of the BST powders as a function of $\frac{1}{2}(\cos^2\theta/\theta+\cos^2\theta/\sin\theta)$. By linearly fitting the data, the extrapolated lattice parameters are obtained at the intersection point of the fitted line and the ordinate axis (as listed in Table S2).[2]

(*hkl*)	BST NPs			BST NCs			BST NRs			BST NWs		
	2θ (°)	*a* (nm)	*c* (nm)	2θ (°)	*a* (nm)	*c* (nm)	2θ (°)	*a* (nm)	*c* (nm)	2θ (°)	*a* (nm)	*c* (nm)
(001)	22.31185	0.39646	0.39812	22.31167	0.39646	0.39812	22.29855	0.39664	0.39835	22.25255	0.39661	0.39917
(100)	22.40656			22.40648			22.39606			22.39806		
(101)	31.80611	0.39672	0.39839	31.80611	0.39674	0.39837	31.78852	0.39680	0.39874	31.75852	0.39684	0.39944
(110)	31.87480			31.87322			31.86805			31.86490		
(002)	45.49455	0.39691	0.39842	45.49055	0.39691	0.39845	45.44152	0.39685	0.39886	45.35855	0.39690	0.39955
(200)	45.67721			45.67711			45.68496			45.67806		
(102)	51.25211	0.39693	0.39858	51.25352	0.39692	0.39857	51.21991	0.39688	0.39888	51.14243	0.39692	0.39958
(201)	51.38912			51.39011			51.38648			51.36219		
(112)	56.58400	0.39696	0.39865	56.58855	0.39698	0.39860	56.55318	0.39692	0.39897	56.47990	0.39696	0.39967
(211)	56.71560			56.71460			56.71243			56.68918		
(202)	66.41082	0.39701	0.39866	66.41082	0.39702	0.39864	66.37717	0.39697	0.39906	66.30817	0.39699	0.39978
(220)	66.56613			66.56403			66.57401			66.57002		

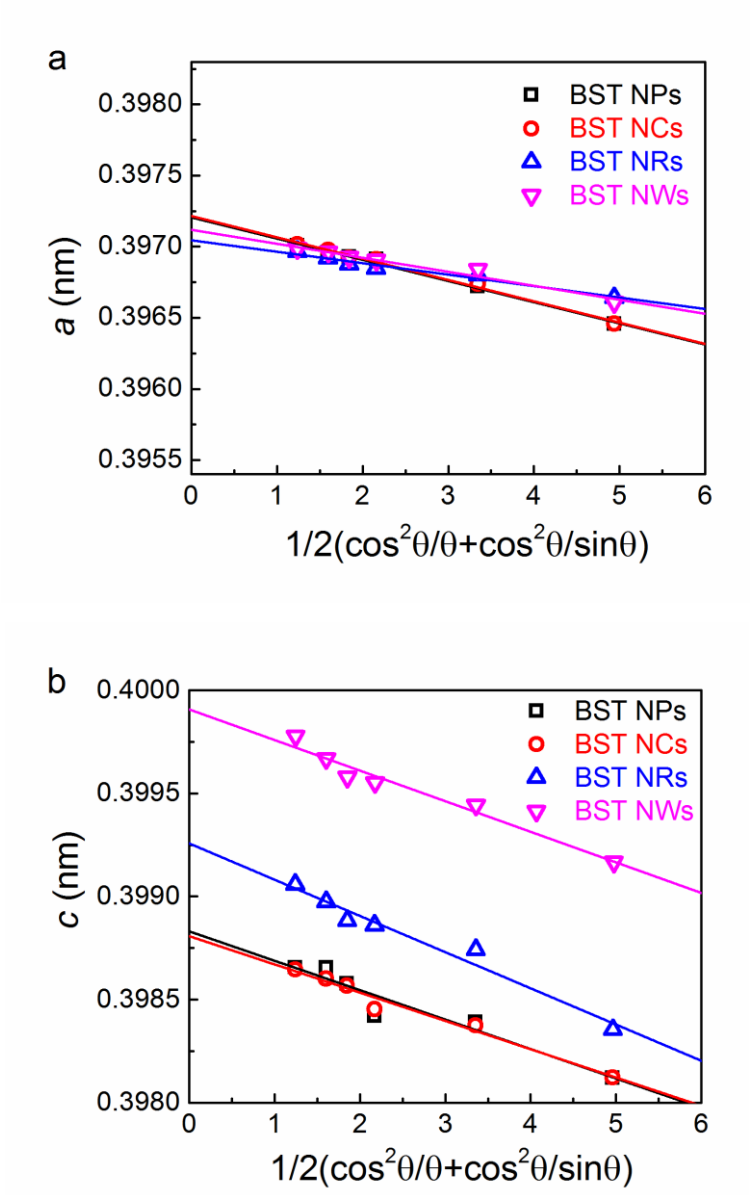

Figure S3. The calculated lattice parameters of the BST powders as a function of ½($\cos^2\theta/\theta + \cos^2\theta/\sin\theta$).

Table S2. Lattice parameters of the BST NPs, NCs, NRs and NWs extrapolated from Figure S3.

BST	*a* [100] (Å)	*c* [001] (Å)	*c*/*a*	Lattice volume (Å^3)
NPs	3.972	3.988	1.004	62.918
NCs	3.972	3.988	1.004	62.918
NRs	3.971	3.993	1.006	62.965
NWs	3.971	3.999	1.007	63.060

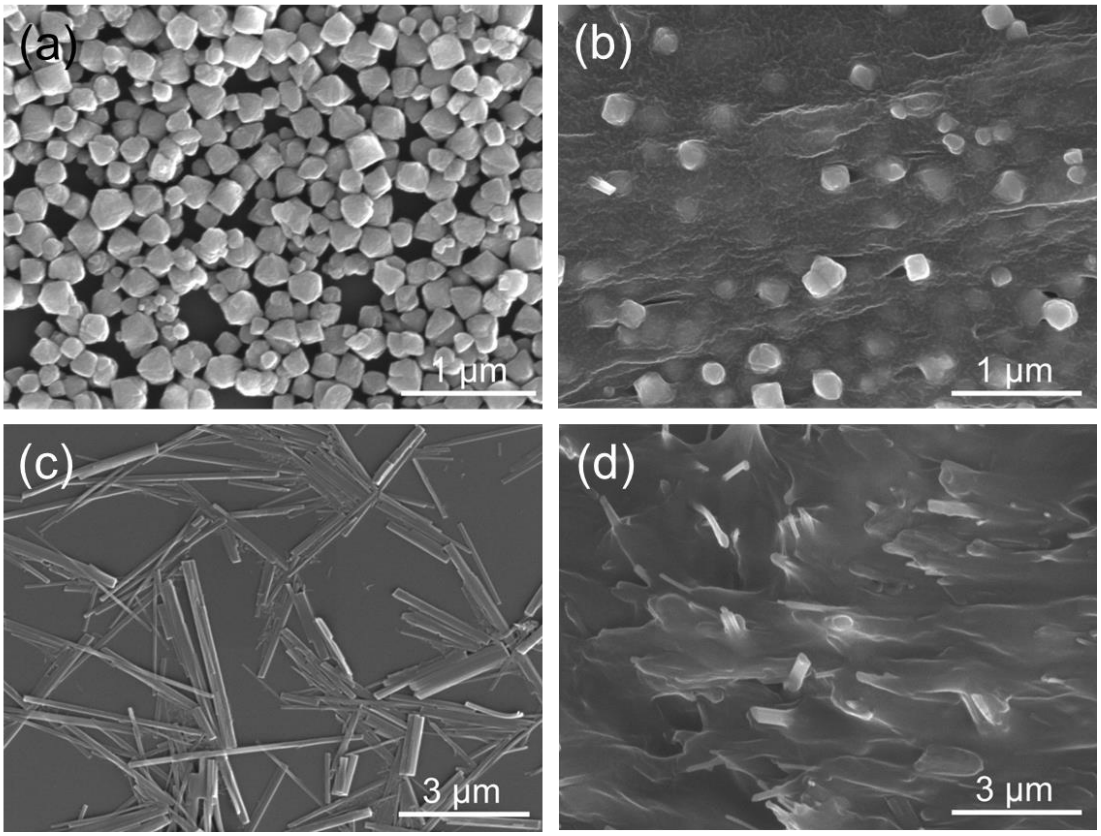

Figure S4. SEM images of the (a) BST NCs and (c) BST NRs. (b) Cross-section SEM image of the P(VDF-TrFE-CFE)/10 vol% BST NCs nanocomposite. (d) Cross-section SEM image of the P(VDF-TrFE-CFE)/10 vol% BST NRs nanocomposite.

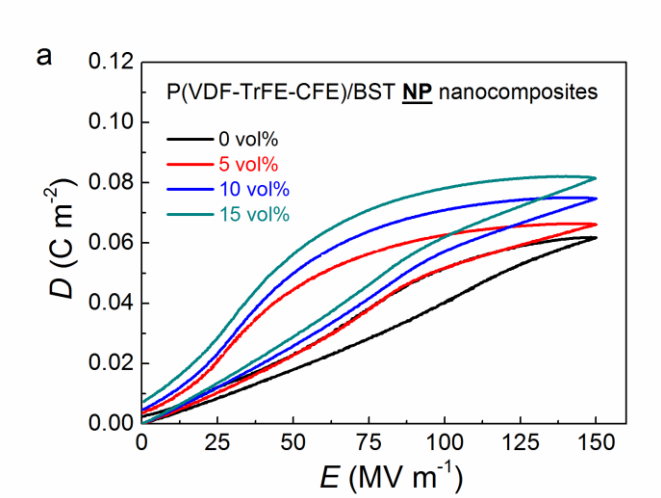
a
P(VDF-TrFE-CFE)/BST NP nanocomposites
0 vol%
5 vol%
10 vol%
15 vol%
D (C m-2)
E (MV m-1)
0.00
0.02
0.04
0.06
0.08
0.10
0.12
0
25
50
75
100
125
150

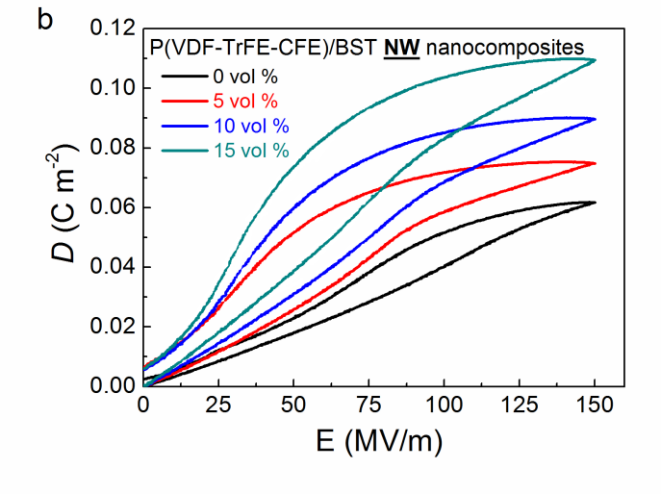
b
P(VDF-TrFE-CFE)/BST NW nanocomposites
0 vol %
5 vol %
10 vol %
15 vol %
D (C m-2)
E (MV/m)
0.00
0.02
0.04
0.06
0.08
0.10
0.12
0
25
50
75
100
125
150

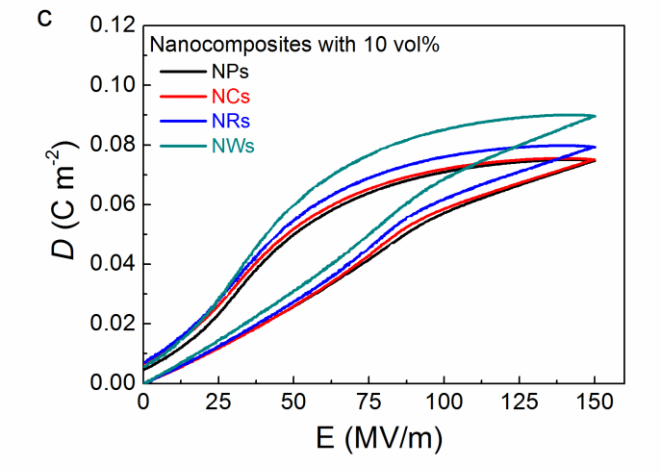
c
Nanocomposites with 10 vol%
NPs
NCs
NRs
NWs
D (C m-2)
E (MV/m)
0.00
0.02
0.04
0.06
0.08
0.10
0.12
0
25
50
75
100
125
150

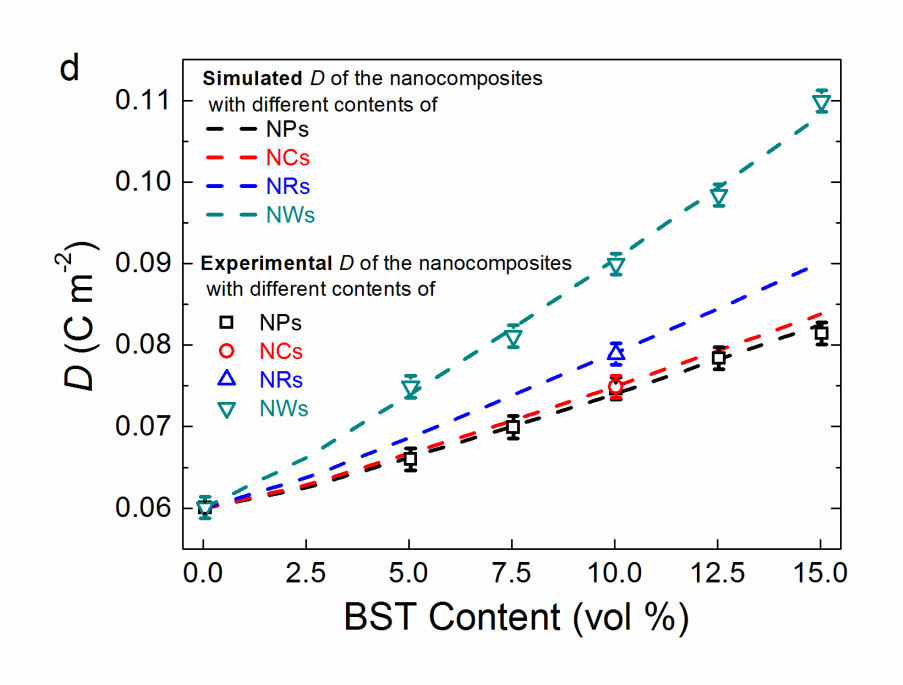

Figure S5. Electric displacement (*D*)-electric field (*E*) loops of the nanocomposites containing different contents of (a) BST NPs and (b) BST NWs. (c) *D*-*E* loops of the nanocomposites with 10 vol% BST NPs, NCs, NRs and NWs. (d) The experimental and phase-field simulated electric displacements of the nanocomposites with different kinds and contents of BST nanofillers. Error bars: Standard error.

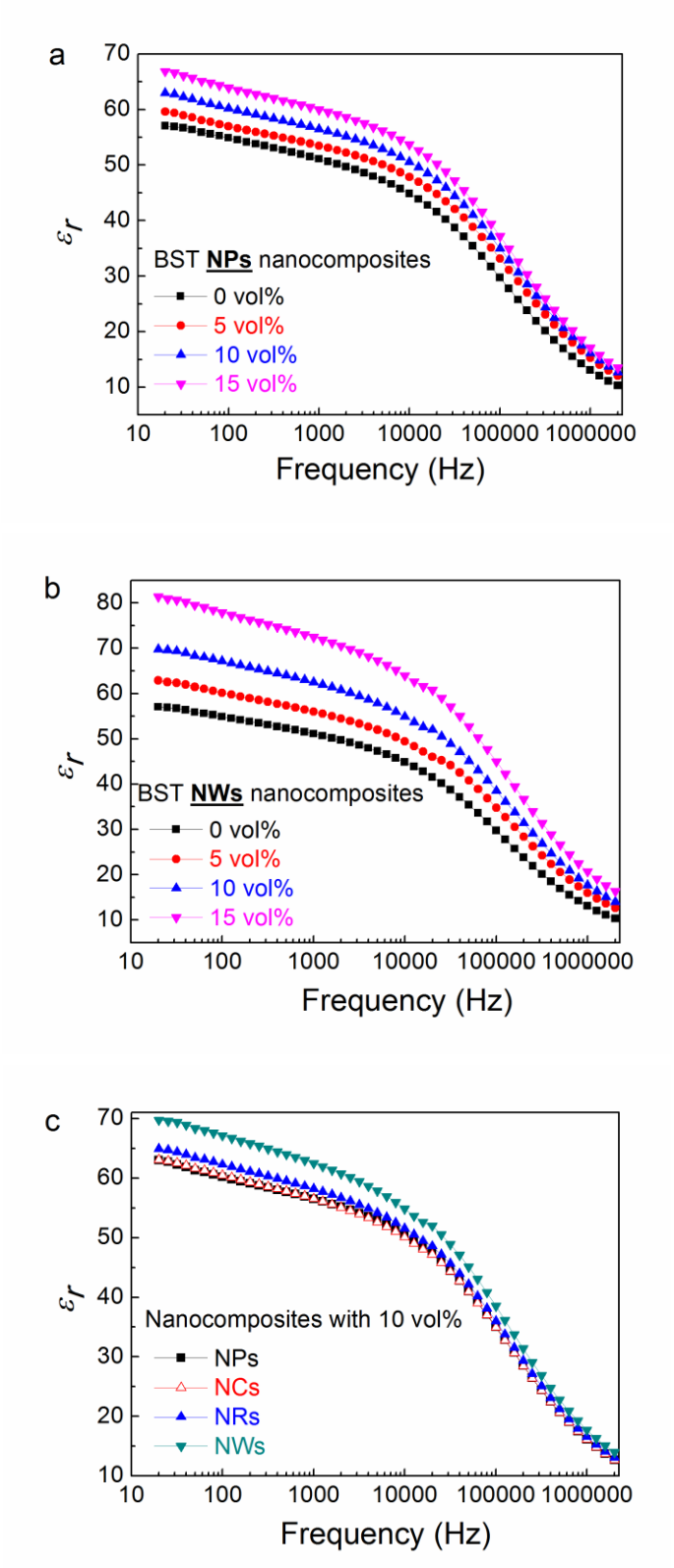

Figure S6. Relative dielectric constant (ε_r) of the nanocomposites with different contents of (a) BST NPs and (b) BST NWs as a function of frequency. (c) Relative dielectric constant-frequency curves of the nanocomposites with 10 vol% BST NPs, NCs, NRs and NWs.

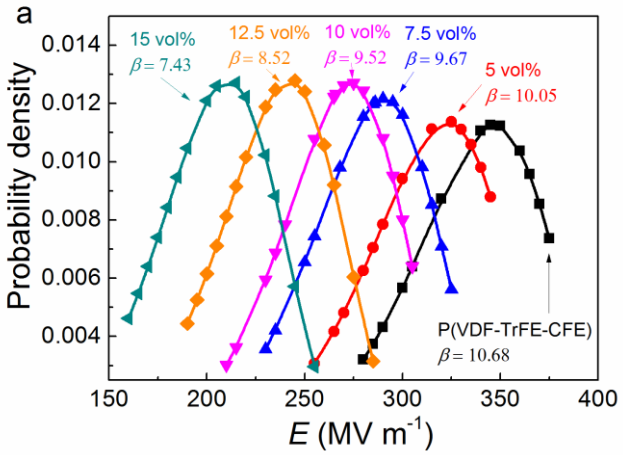
a
15 vol%
β = 7.43
12.5 vol%
β = 8.52
10 vol%
β = 9.52
7.5 vol%
β = 9.67
5 vol%
β = 10.05
P(VDF-TrFE-CFE)
β = 10.68
Probability density
E (MV m-1)

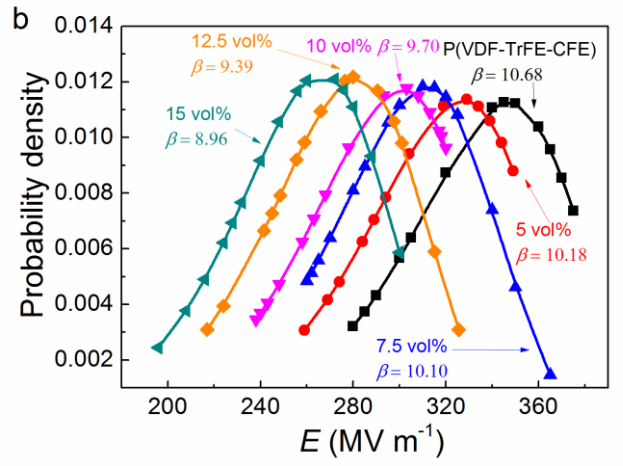
b
12.5 vol%
β = 9.39
10 vol% β = 9.70
P(VDF-TrFE-CFE)
β = 10.68
15 vol%
β = 8.96
5 vol%
β = 10.18
7.5 vol%
β = 10.10
Probability density
E (MV m-1)

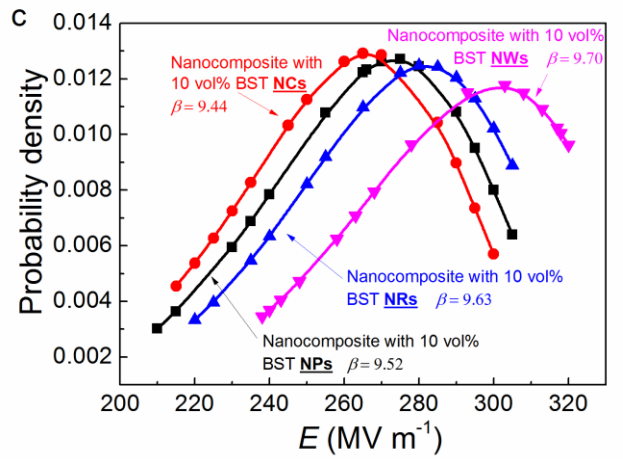
c
Nanocomposite with 10 vol%
BST NWs β = 9.70
Nanocomposite with
10 vol% BST NCs
β = 9.44
Nanocomposite with 10 vol%
BST NRs β = 9.63
Nanocomposite with 10 vol%
BST NPs β = 9.52
Probability density
E (MV m-1)

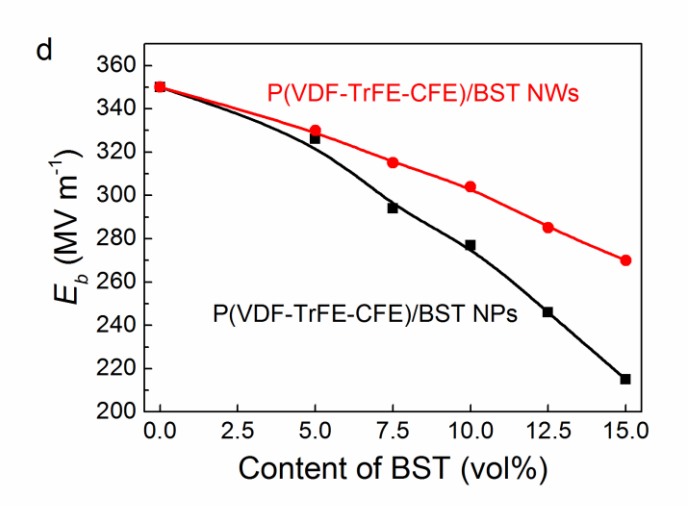

Figure S7. Weibull plots of the (a) P(VDF-TrFE-CFE)/BST NPs and (b) P(VDF-TrFE-CFE)/BST NWs nanocomposites. (c) Weibull plots of the nanocomposites with 10 vol% BST NPs, NCs, NRs and NWs. (d) Weibull breakdown strength (E_b) of the P(VDF-TrFE-CFE)/BST nanocomposites as a function of BST content.

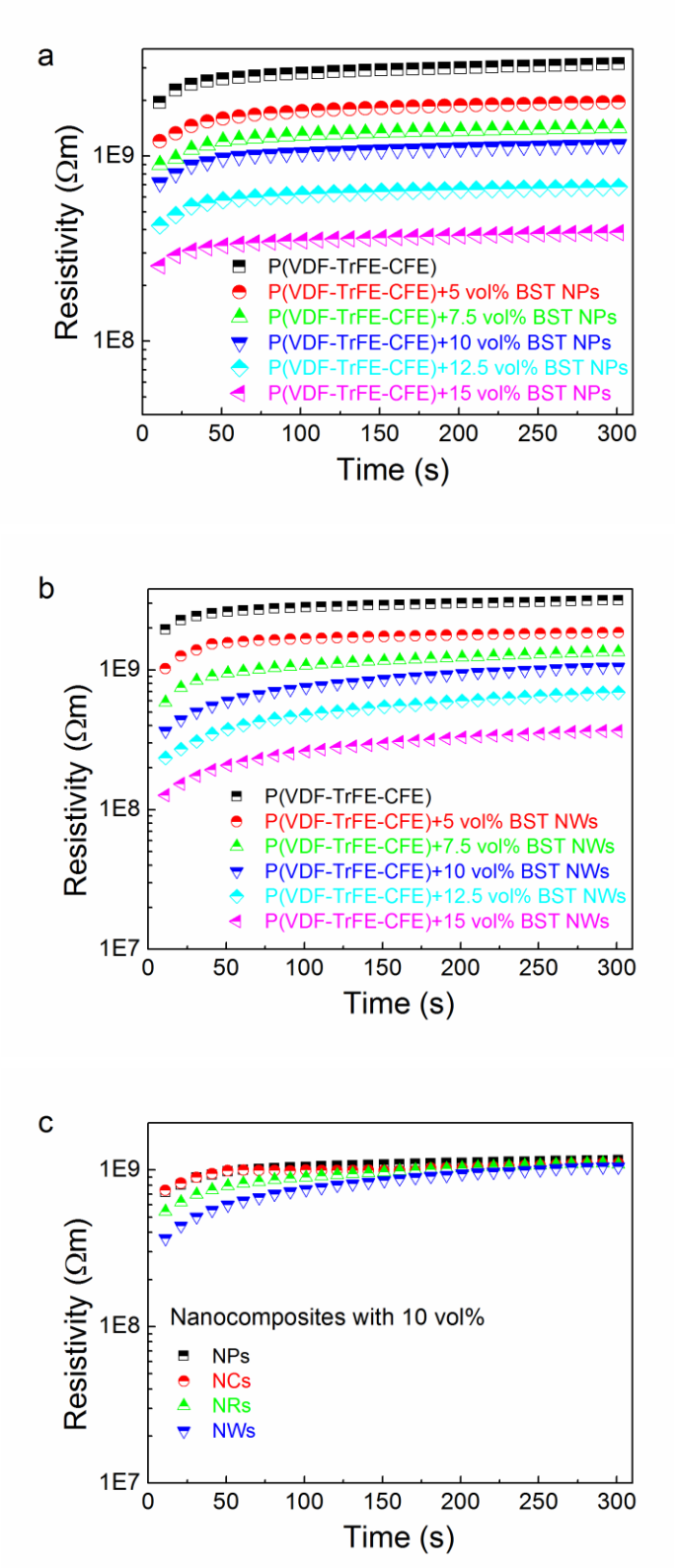
a
Resistivity (Ωm)
1E9
1E8
0
50
100
150
200
250
300
Time (s)
P(VDF-TrFE-CFE)
P(VDF-TrFE-CFE)+5 vol% BST NPs
P(VDF-TrFE-CFE)+7.5 vol% BST NPs
P(VDF-TrFE-CFE)+10 vol% BST NPs
P(VDF-TrFE-CFE)+12.5 vol% BST NPs
P(VDF-TrFE-CFE)+15 vol% BST NPs
b
Resistivity (Ωm)
1E9
1E8
1E7
0
50
100
150
200
250
300
Time (s)
P(VDF-TrFE-CFE)
P(VDF-TrFE-CFE)+5 vol% BST NWs
P(VDF-TrFE-CFE)+7.5 vol% BST NWs
P(VDF-TrFE-CFE)+10 vol% BST NWs
P(VDF-TrFE-CFE)+12.5 vol% BST NWs
P(VDF-TrFE-CFE)+15 vol% BST NWs
c
Resistivity (Ωm)
1E9
1E8
1E7
0
50
100
150
200
250
300
Time (s)
Nanocomposites with 10 vol%
NPs
NCs
NRs
NWs

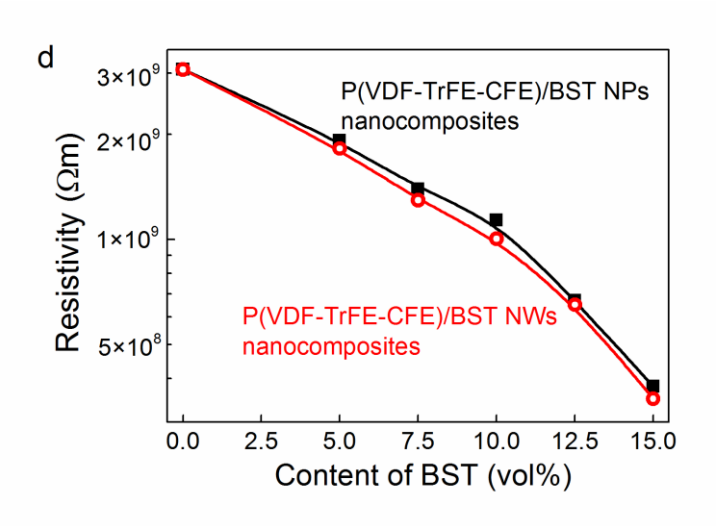

Figure S8. Time dependence of electrical resistivity of the (a) P(VDF-TrFE-CFE)/BST NPs and (b) P(VDF-TrFE-CFE)/BST NWs nanocomposites. (c) Time dependence of electrical resistivity of the nanocomposites with 10 vol% BST NPs, NCs, NRs and NWs. (d) Electrical resistivity of the P(VDF-TrFE-CFE)/BST nanocomposites as a function of filler content.

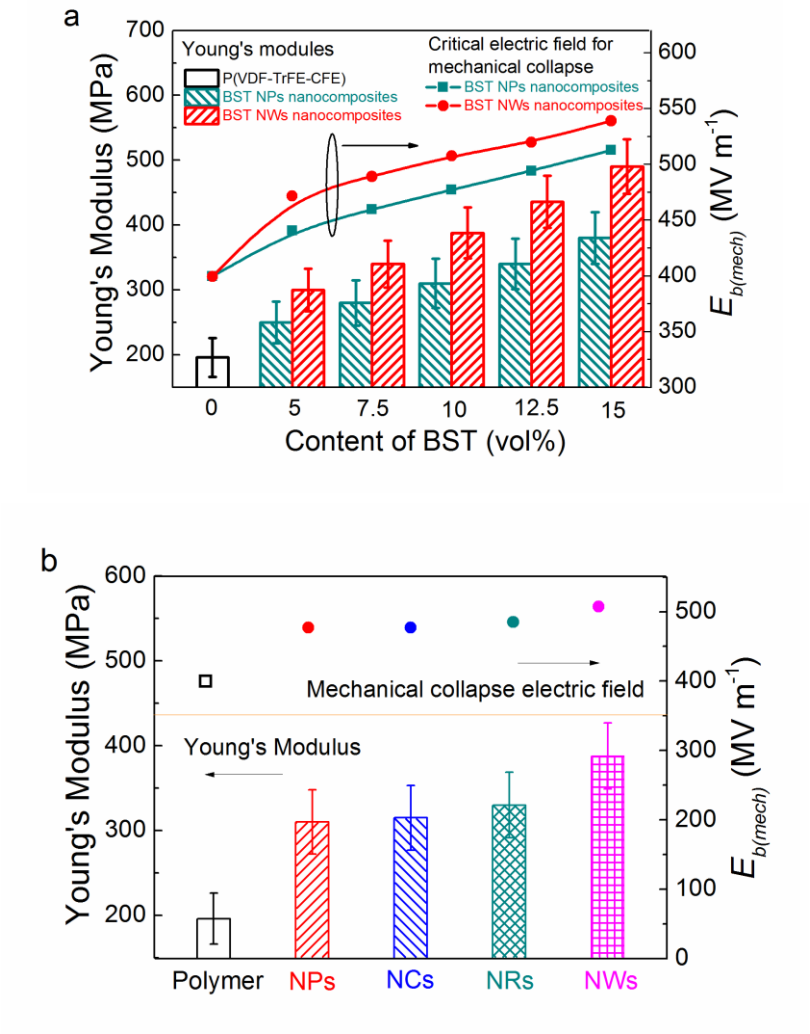

Figure S9. Young's modulus and critical mechanical collapse electric fields calculated according to Equation 5 of the nanocomposites. (a) The nanocomposites containing different contents of BST NPs and NWs. (b) The P(VDF-TrFE-CFE) and its nanocomposites with 10 vol% BST NPs, NCs, NRs and NWs. Error bars: Standard error.

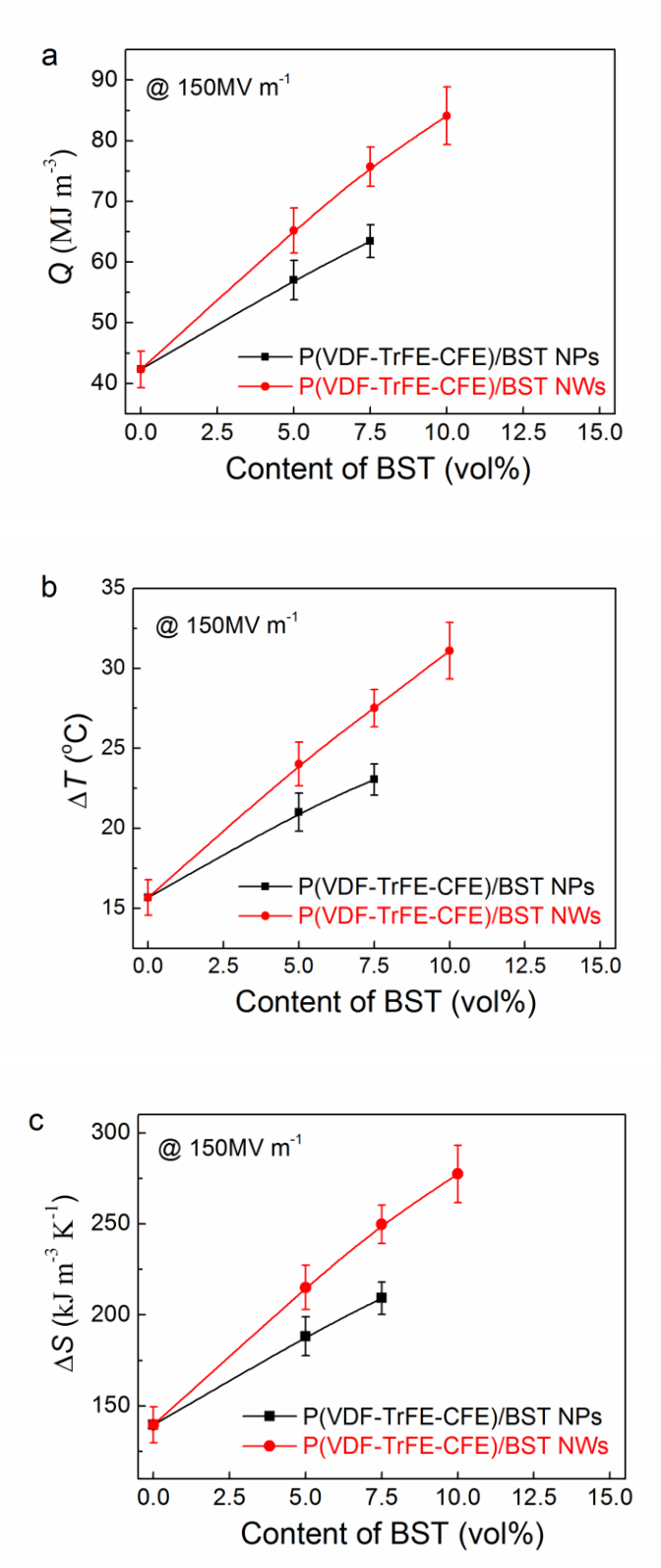

Figure S10. (a) *Q*, (b) Δ*T* and (c) Δ*S* of the P(VDF-TrFE-CFE) and nanocomposites with different contents of BST NPs and NWs at 150 MV m^{-1}. Error bars: Standard error.

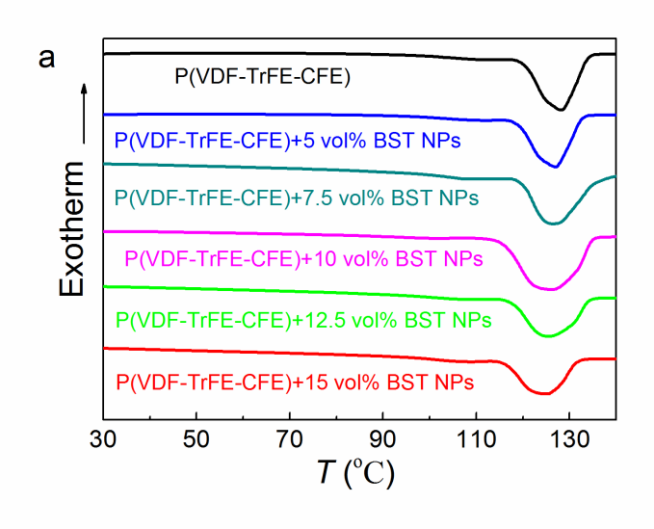
a
P(VDF-TrFE-CFE)
P(VDF-TrFE-CFE)+5 vol% BST NPs
P(VDF-TrFE-CFE)+7.5 vol% BST NPs
P(VDF-TrFE-CFE)+10 vol% BST NPs
P(VDF-TrFE-CFE)+12.5 vol% BST NPs
P(VDF-TrFE-CFE)+15 vol% BST NPs
Exotherm
30
50
70
90
110
130
T (°C)

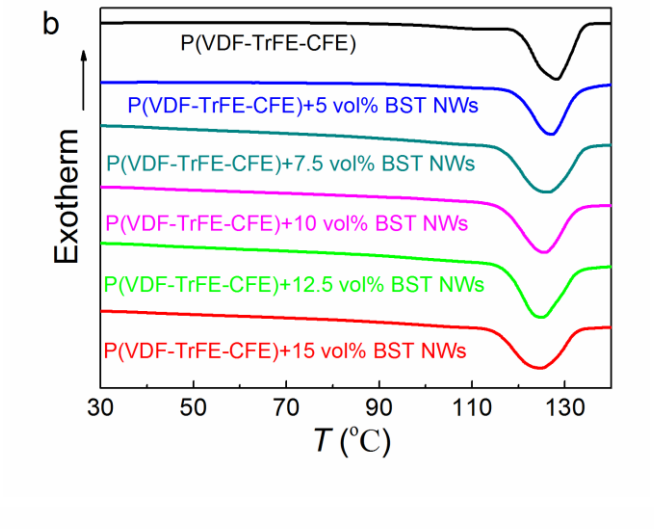
b
P(VDF-TrFE-CFE)
P(VDF-TrFE-CFE)+5 vol% BST NWs
P(VDF-TrFE-CFE)+7.5 vol% BST NWs
P(VDF-TrFE-CFE)+10 vol% BST NWs
P(VDF-TrFE-CFE)+12.5 vol% BST NWs
P(VDF-TrFE-CFE)+15 vol% BST NWs
Exotherm
30
50
70
90
110
130
T (°C)

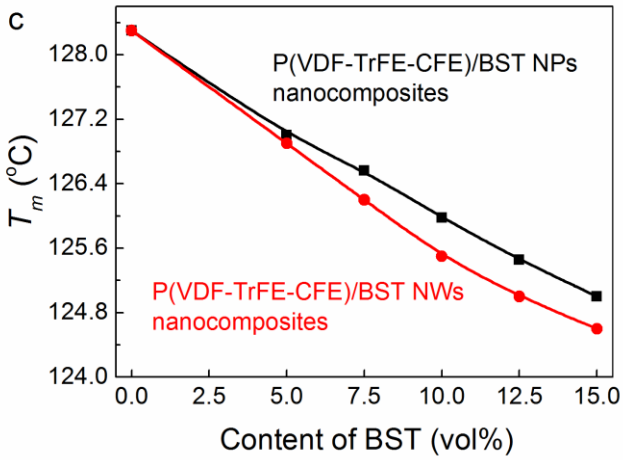
c
P(VDF-TrFE-CFE)/BST NPs
nanocomposites
P(VDF-TrFE-CFE)/BST NWs
nanocomposites
T_m (°C)
128.0
127.2
126.4
125.6
124.8
124.0
0.0
2.5
5.0
7.5
10.0
12.5
15.0
Content of BST (vol%)

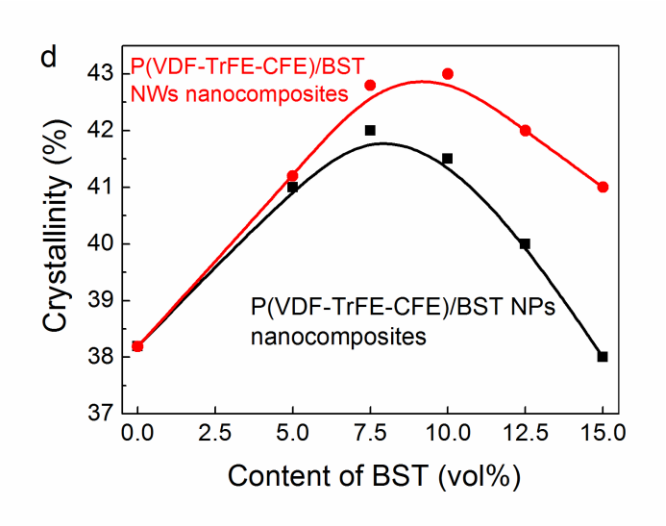

Figure S11. DSC profiles of the (a) P(VDF-TrFE-CFE)/BST NPs and (b) P(VDF-TrFE-CFE)/BST NWs nanocomposites. (c) The melting temperatures (T_m) and (d) degree of crystallinity derived from the DSC profiles. T_m of the nanocomposites decreases as the content of BST increases, indicating that the presence of the nanoparticles in the polymer matrix decreases the crystal size of the terpolymer. This has been further confirmed by the XRD studies shown in Figure S12. In addition, the crystallinity increases as the content of BST increases up to 7.5 vol% for the P(VDF-TrFE-CFE)/BST NPs nanocomposites and 10 vol% for the P(VDF-TrFE-CFE)/BST NWs nanocomposites. The crystallinity was calculated from $\Delta H^0_{f,PVDF}$=104.7 J/g corresponding to the heat of formation of PVDF with theoretical 100% crystalline. It should be noted that the T_m of the P(VDF-TrFE-CFE)/BST NWs nanocomposites is lower, whereas the degree of crystallinity is higher than those of P(VDF-TrFE-CFE)/BST NPs nanocomposites when the same content of BST is added.

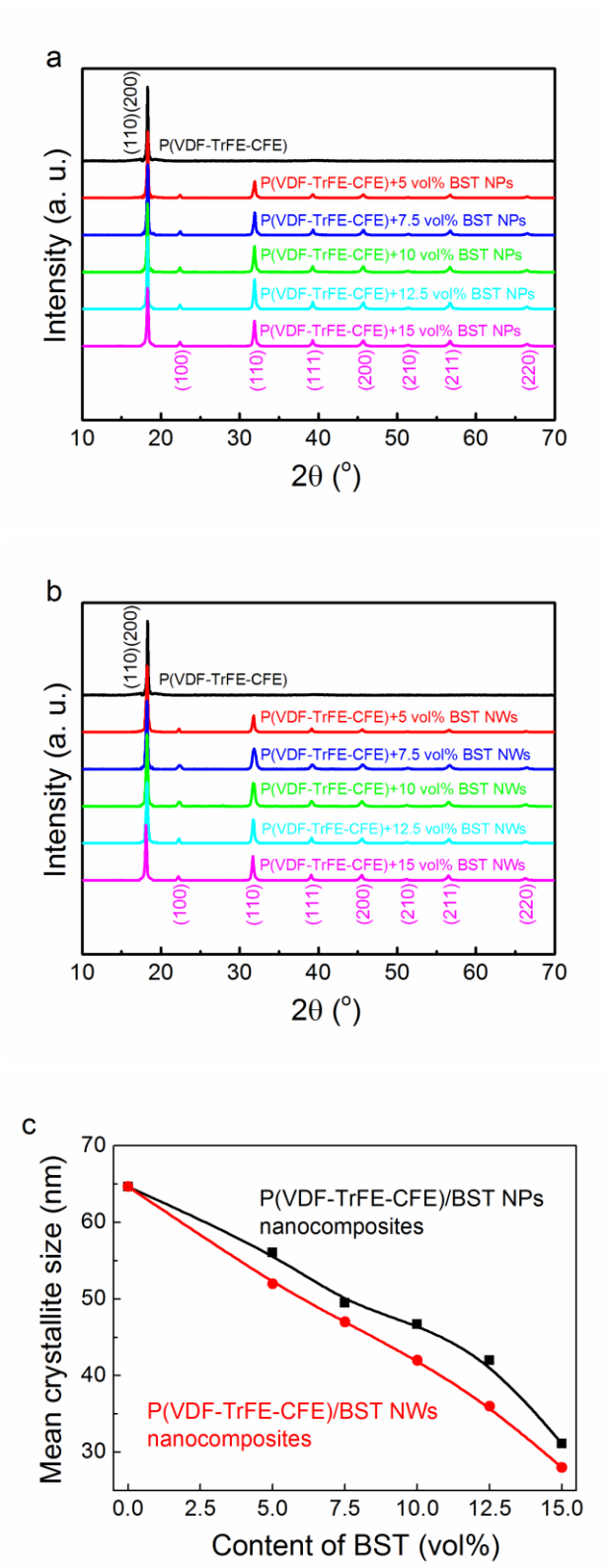

Figure S12. XRD patterns of the (a) P(VDF-TrFE-CFE)/BST NPs and (b) P(VDF-TrFE-CFE)/BST NWs nanocomposites. (c) Calculation of mean crystallite sizes for (110)/(200) face of P(VDF-TrFE-CFE) and P(VDF-TrFE-CFE)/BST polymer nanocomposites. The mean crystallite sizes of the nanocomposites decreases

as the content of BST increases, especially for the nanocomposites with BST NWs.

The calculation of mean crystallite size is based on the Scherrer equation $\tau=(r\lambda)/\beta\cos\theta$, where τ is the mean size of the crystalline domains, r is a dimensionless shape factor, λ is the X-ray wavelength, β is the line broadening at half the maximum intensity (FWHM), and θ is the Bragg angle.

References

1. Takeuchi, T.; Tabuchi, M.; Kageyama, H. Preparation of Dense $BaTiO_3$ Ceramics with Submicrometer Grains by Spark Plasma Sintering. *J. Am. Ceram. Soc*. **1999**, 82, 939-943.
2. Nelson, J. B.; Riley, D. P. An Experimental Investigation of Extrapolation Methods in the Derivation of Accurate Unit-Cell Dimensions of Crystals, *Proc. Phys. Soc*. **1945**, *57*, 160-176.